Arabian Journal for Science and Engineering
https://doi.org/10.1007/s13369-020-04679-0

RESEARCH ARTICLE-MECHANICAL ENGINEERING

Optimization of Milling Parameters for Energy Savings and Surface Quality

Trung-Thanh Nguyen[1] · **Truong-An Nguyen**[2] · **Quang-Hung Trinh**[2]

Received: 29 May 2019 / Accepted: 29 May 2020

Abstract
Enhancing energy efficiency and product quality by means of optimal inputs is a cost-effective solution, as compared to the drastic investment. This paper aims to optimize the machining inputs to enhance energy efficiency (EF) as well as the power factor (PO) and decrease the surface roughness (R_a) for the milling process. The factors considered are the feed (f), depth of cut (a), milling speed (V), and tool radius (r). The machining operations were executed on the vertical milling under the dry condition for the stainless steel 304. A type of neutral network entitled the radius basic function (RBF) was used to render the relationships between milling inputs and performances measured. The adaptive simulated annealing (ASA) algorithm was applied to obtain the optimal values. The outcomes indicated that the milling responses are primarily influenced by a, f, V, and r, respectively. The reduction in R_a is approximately 39.18%, while the improvements in EF and PO are around 22.61% and 26.47%, respectively, as compared to the initial parameter settings. The explored findings are expected as a prominent solution for the industrial application of the dry machining. The combination of the RBF models and ASA could be considered as an efficient approach for modeling dry machining processes and generating reliable as well as feasible optimal results.

Keywords Energy efficiency · Surface roughness · Optimization · Milling, parameters · ASA

1 Introduction

The dry machining is an effective solution to decrease the manufacturing costs as well as environmental impacts and protect the worker's health. The lubrication used in the machining process is an unsustainable factor, which has negative influences on environmental safety and human. The air pollution generated by the usage of lubrication may cause some problems in the operator's skin and lungs. The lubrication cost is around 7–17% of the tool cost [1]. The dry machining is a prominent approach to remove the negative impacts of the lubrication, as compared to the traditional one. The concept of sustainable machining is associated with high energy efficiency, low environmental issues, more effective material flow, and low health safety. Therefore, the machining operation employing the dry condition is an intelligent approach to achieve sustainable manufacturing.

The machining responses under the dry condition have been explored in the published works. The fuzzy system (FS) was applied to develop the correlations between the inputs and roughness as well as cutting temperature [2]. Shihab et al. used the response surface method (RSM) to analyze the surface roughness for the dry turning of the hardened steel [3]. Similarly, the RSM and FS were applied to forecast the roughness value [4]. The Taguchi-based approach was used to minimize the turning forces and surface properties for the Inconel [5] and AISI D3 materials [6]. The assessments of the machining performances under the dry and minimum lubrication conditions were presented in the work of [7]. The formulation of the tool life for the milled titanium was proposed by means of the FS [8]. Karabulut et al. stated that the neural network (NN) is more efficient than the regression analysis for forecasting roughness of the milled composite [9]. Li et al. analyzed the tool wear and hole quality for the helical milling of Ti–6Al–4V alloy [10]. The temperature variation in the workpiece and cutting tool was investigated for the dry milling of Inconel 718 [11]. The optimizing issues were solved to enhance surface properties for milling

✉ Trung-Thanh Nguyen
trungthanhk21@mta.edu.vn;
nguyentrungthanh6@duytan.edu.vn

[1] Institute of Research and Development, Duy Tan University, 03 Quang Trung, Da Nang 550000, Vietnam

[2] Faculty of Mechanical Engineering, Le Quy Don Technical University, 236 Hoang Quoc Viet, Hanoi 100000, Vietnam

Published online: 11 June 2020

operations of the magnesium alloy [12], aluminum [13], and Ti–6Al–4V alloy [14]. The improvements in the roughness and hardness of the milled magnesium alloy were obtained employing the optimal factors [15]. The Taguchi-based approach was applied to optimize machining parameters in terms of the cutting force and tool wear [16]. The effects of the helix angle and cutting tool characteristics on the surface roughness and tool life were examined by Baowan et al. [17]. The RSM was applied to analyze the impacts of cutting parameters on energy consumption for the dry milling process of carbon steel [18]. An energy-used model was proposed for the face milling process [19]. Zhang et al. proposed the correlations between the inputs and the processing time, specific energy used, and carbon emissions [20].

As a result, the technological responses, including surface characteristics, tool life, machining forces, machined power, and energy used, were considered as the objectives of the different dry machining operations. However, the energy efficiency of the dry milling process has not been thoroughly presented in the published works. Moreover, the power factor of the machining system also has a significant contribution to energy savings [21]. Additionally, the selection of optimal inputs for improving energy efficiency and roughness of the milled part has not been considered in the aforementioned works.

In this paper, the correlations between milling conditions and energy efficiency (EF), power factor (PO), and roughness (R_a) were generated. The ANOVA results are used to assess the statistical significance of the proposed models and factors. The adaptive simulated annealing (ASA) algorithm is utilized to predict the optimal parameters.

2 Methodology

The optimization procedure of the milling process is shown in Fig. 1a. The sequential steps are listed as follows:

Step 1 A set of milling trails is performed to obtain the experimental data [22].

Step 2 The predictive models of EF, PF, and R_a are constructed using the RBF models. For the RBF correlations, the radial basis function is the active approximation. The output is a complex combination of the radial and linear units. The primary advantages of the RBF models are fast training, compact system, and high computational efficiency [23]. RBF approximations are useful in approximating a wide range of nonlinear spaces. The RBF model is expressed using Eq. 1:

$$F(x) = \sum_{i=1}^{n} \lambda_i \phi\left(\left(x - x_i\right)\right) + bx + c \tag{1}$$

where λ_i, b, and c are the parameters to be determined, which are obtained by the equations in the matrix form:

$$\begin{bmatrix} \phi & P \\ P^T & 0 \end{bmatrix} \begin{Bmatrix} \lambda \\ a \end{Bmatrix} = \begin{Bmatrix} F \\ 0 \end{Bmatrix} \tag{2}$$

$$P = \begin{Bmatrix} 1 & X_1^{\mathrm{T}} \\ 1 & X_2^{\mathrm{T}} \\ . & . \\ . & . \\ . & . \\ 1 & X_n^{\mathrm{T}} \end{Bmatrix}, \ \lambda = \begin{Bmatrix} \lambda_1 \\ \lambda_2 \\ . \\ . \\ . \\ \lambda_n \end{Bmatrix}, \ a = \begin{Bmatrix} c \\ b_1 \\ b_2 \\ . \\ . \\ b_d \end{Bmatrix}, \ b = \begin{Bmatrix} b_1 \\ b_2 \\ . \\ . \\ . \\ b_d \end{Bmatrix}, \ F = \begin{Bmatrix} f(x_1) \\ f(x_2) \\ . \\ . \\ . \\ f(x_2) \end{Bmatrix} \tag{3}$$

where ϕ and d are the $n \times n$ matrix and the dimension of vector x.

In the current paper, the multi-quadratic form is used to improve the prediction accuracy and expressed as:

$$\phi(r) = \sqrt{r^2 + \gamma^2} \tag{4}$$

where γ is the positive coefficient.

Step 3 ANOVA is conducted to investigate the statistical significance of the inputs.

Step 4 Determine optimal parameters using the adaptive simulated annealing (ASA) algorithm. The ASA algorithm is an efficient technique, which is well suited to solve highly nonlinear problems with minimal running time. During the computational time, the heating temperature is gradually dropped to decrease the defects. The new solution is obtained with the support of the annealing function. The probability scatter is presented by the currently processed temperature. The reduction in the temperature leads to a wider design space and ensures the global solution. The operating algorithm of the ASA is listed as below (Fig. 1b):

- The start solution (α^{init}) having parameter values is selected in the random space. The values of the anneal time ka and kg_i are equal to zero. The value of the initial temperature TA (ka) is set to $f(\alpha^{\mathrm{init}})$. The initial generated temperature TG_i (kg_i) is set to 1.
- A new point is generated using Eq. 5:

$$\alpha_i^{\mathrm{new}} = \alpha_i^{\mathrm{old}} + y_i\left(B_i - A_i\right), \quad i = 1 \ldots D \tag{5}$$

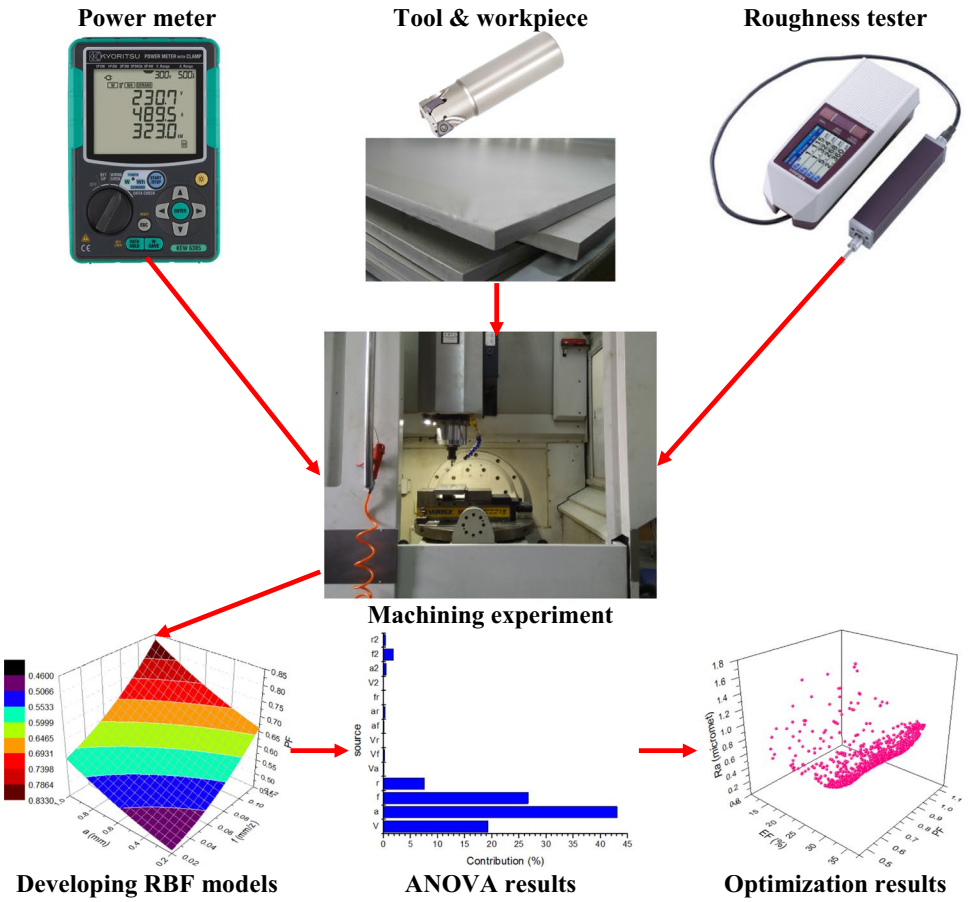

(a) Optimization procedure

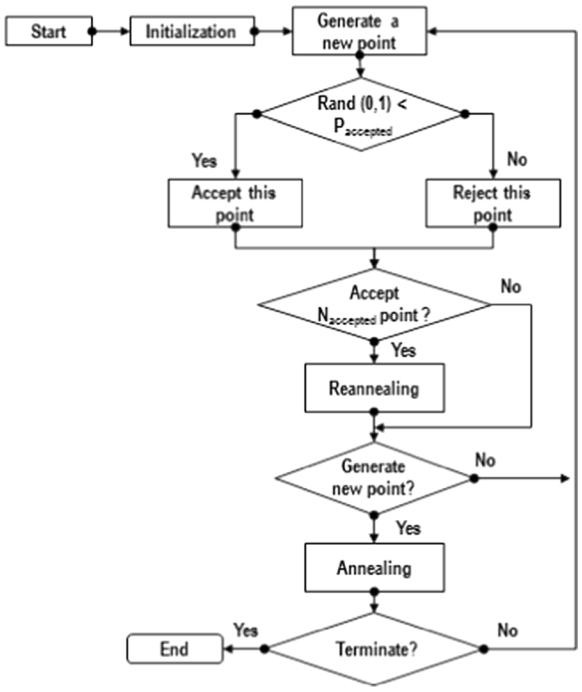

(b) Operating procedure of the ASA

Fig. 1 Optimization approach for generating optimal values

where B_i and A_i denote the lower and upper inputs. Y_i is a resulting form in the u_i space ($u_i \in [0, 1]$) and expressed as:

$$y_i = \mathrm{sgn}(u_i - 0.5) TG_i(kg_i) \times \left(\left[1 + \frac{1}{TG_i(kg_i)} \right]^{|2u_i - 1|} - 1 \right). \tag{6}$$

- The acceptable point is identified using Eq. 7:

$$P_{\text{accept}} = \frac{1}{1 + \exp^{\frac{f(\alpha^{\text{new}}) - f(\alpha^{\text{old}})}{TA(k\alpha)}}} \tag{7}$$

- The re-annealing process is conducted to estimate the sensitive value of the accepted point.

$$s_i = \left| \frac{F\left(\alpha^{\text{best}} + \left(\eta \alpha^{\text{best}} \times e_i\right) - F\left(\alpha^{\text{best}}\right)\right.}{\eta \alpha^{\text{best}} \times e_i} \right| \tag{8}$$

where α^{best}, η, and e_i present the best point, small step size, and dimensional vector of ith element. The values of the generated temperature and annealing time are also updated.

$$TG_i(kg_i) = \frac{S_{\max}}{S_i} TG_i(kg_i) \tag{9}$$

$$kg_i = \left(\frac{1}{c} \ln \left(\frac{TG_i(0)}{TG_i(kg_i)} \right) \right) \tag{10}$$

$$ka = \left(\frac{1}{c} \ln \left(\frac{TA(0)}{TA(ka)} \right) \right) \tag{11}$$

- The algorithm will be stopped if the ASA accepts the newly generated points. In contrast, the procedure returns to step 2.

3 Experiments and Measurements

The workpiece is a SS 304, which is clamped on the machine table employing the precision vise. The machining specimen is prepared in dimensions of 350 mm × 150 mm × 25 mm. The workpiece is machined using the grinding process to enhance the dimensional accuracy.

The up-milling tests are conducted with the support of a vertical milling machine under dry machining conditions. A standard 12-mm tool shank with two quality wiper inserts is used in the experiments. The milling slot is machined with a new insert with different combinations of the factors.

Power Meter KEW6305 is used to record the consumed powers and the power factor at different stages. The experimental data obtained are transferred to a personal computer and visualized with the help of the offline software.

The energy efficiency of the milling process (EF) is defined as the ratio of the cutting energy consumption (CEC) to the energy consumption by the machine (ECM) in the cutting time. The value of EF is calculated using Eq. 12:

$$\mathrm{EF} = \frac{\mathrm{CEC}}{\mathrm{ECM}} = \frac{\mathrm{ACP} \times t_{\mathrm{m}}}{\mathrm{PCM} \times t_{\mathrm{m}}} = \frac{\mathrm{ACP}}{\mathrm{CPM}} \tag{12}$$

where ACP, CPM, and t_{m} denote the active cutting power, power consumed by machine, and milling time, respectively.

The power factor (PO) is defined as the ratio of the active power (AP) to the apparent power (APP):

$$\mathrm{PO} = \frac{\mathrm{AP}}{\mathrm{APP}} = \frac{\mathrm{AP}}{\sqrt{\mathrm{AP}^2 + \mathrm{RP}^2}} \tag{13}$$

where RP denotes the reactive power.

A tester Mitutoyo SJ-301 is used to measure the surface roughness at five different positions. The roughness is taken according to standard ISO 4287. The average value of the R_a is calculated using Eq. 14:

$$R_a = \frac{R_{a1} + R_{a2} + R_{a3} + R_{a4} + R_{a5}}{5} \tag{14}$$

The parameters considered are the cutting speed V, depth of cut a, feed rate f, and nose radius r. The levels of machining factors are shown in Table 1. The parameter ranges are determined based on a user guide of the manufacturer and common values used in the automotive industry. The milling trails are conducted at the highest levels of inputs to ensure the allowable power of the spindle motor.

The values of PO at various inputs are shown in Fig. 2. The representative values of the power consumed by the machine tool at different conditions are depicted in Fig. 3. The values of the R_a at different conditions are shown in Fig. 4.

Table 1 Processing conditions

Symbol	Parameters	level − 1	level 0	level + 1
V	Cutting speed (m/min)	80	120	160
a	Depth of cut (mm)	0.4	0.8	1.2
f	Feed rate (mm/z)	0.03	0.07	0.1
r	Nose radius (mm)	0.2	0.4	0.8

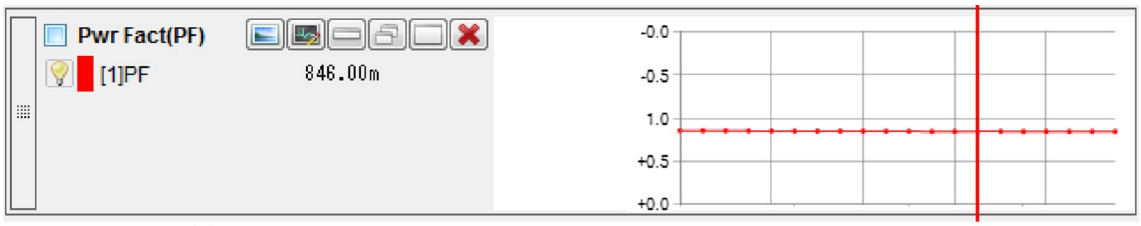

(a) The value of the *PO* at the experimental No. 1 (Replication-2)

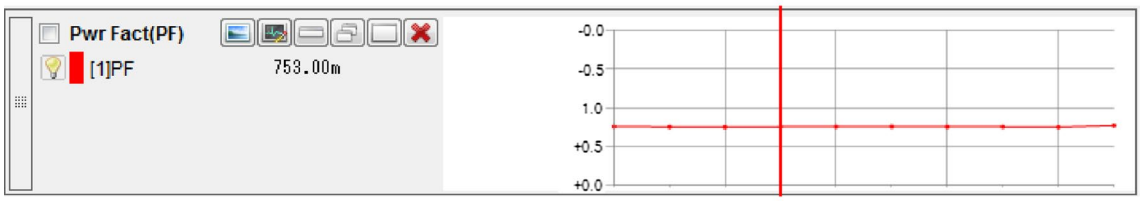

(b) The value of the *PO* at the experimental No. 3 (Replication-3)

Fig. 2 The values of PO at different inputs

Fig. 3 The values of the power consumed by the machine tool at different inputs

(a) The value of the power consumed by the machine tool at the experimental No. 20 (Replication-2)

(b) The value of the power consumed by the machine tool at the experimental No. 7 (Replication-3)

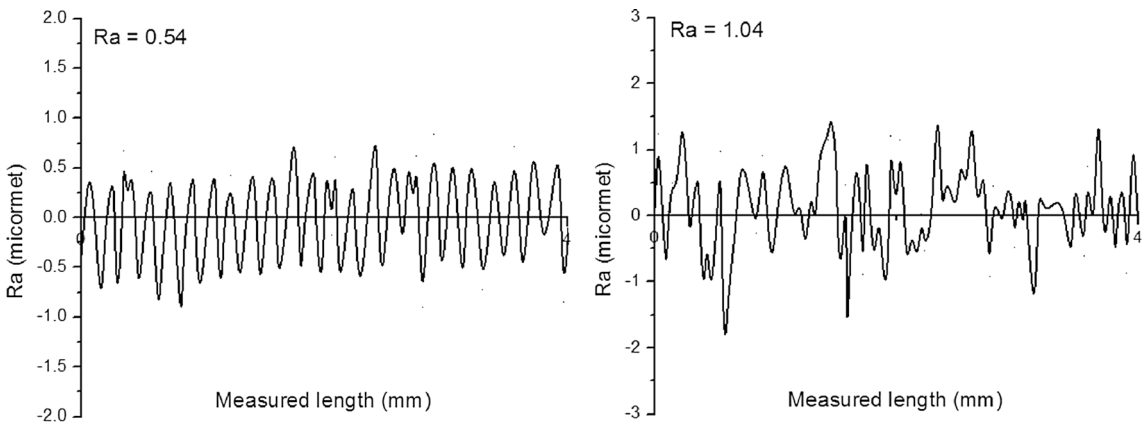

(a) The value of the roughness at the experimental No. 19 (Replication-2)

(b) The value of the roughness at the experimental No. 6 (Replication-3)

Fig. 4 The values of the roughness at different inputs

Table 2 Experimental results

No.	V (m/min)	a (mm)	f (mm/z)	r (mm)	PO	EF (%)	R_a (μm)
1	120	1.2	0.07	0.8	0.846	29.89	1.21
2	120	0.4	0.1	0.4	0.661	20.35	1.09
3	120	0.8	0.1	0.2	0.753	23.97	1.63
4	80	1.2	0.07	0.4	0.736	25.44	1.48
5	160	0.4	0.07	0.4	0.675	21.96	0.51
6	160	1.2	0.07	0.4	0.817	30.24	1.03
7	120	1.2	0.03	0.4	0.699	22.77	1.26
8	120	0.8	0.03	0.2	0.611	16.29	1.14
9	120	1.2	0.1	0.4	0.828	29.26	1.69
10	120	0.8	0.03	0.8	0.707	20.02	0.76
11	160	0.8	0.03	0.4	0.691	19.71	0.73
12	120	0.4	0.07	0.2	0.596	17.92	0.89
13	160	0.8	0.1	0.4	0.801	27.49	1.36
14	80	0.8	0.03	0.4	0.572	14.76	1.06
15	80	0.8	0.1	0.4	0.711	20.54	1.52
16	80	0.8	0.07	0.8	0.719	22.51	0.96
17	120	0.4	0.03	0.4	0.542	12.78	0.59
18	120	0.8	0.07	0.4	0.681	22.14	0.97
19	160	0.8	0.07	0.8	0.839	28.64	0.53
20	160	0.8	0.07	0.2	0.741	24.81	0.93
21	120	0.4	0.07	0.8	0.702	22.32	0.57
22	80	0.8	0.07	0.2	0.647	18.77	1.39
23	120	0.8	0.1	0.8	0.835	26.79	1.32
24	80	0.4	0.07	0.4	0.556	15.62	0.82
25	120	1.2	0.07	0.2	0.764	27.74	1.58
26	120	1.2	0.07	0.8	0.846	29.89	1.21
27	120	0.4	0.1	0.4	0.661	20.05	1.09
28	120	0.8	0.1	0.2	0.753	23.97	1.63
29	80	1.2	0.7	0.4	0.736	25.44	1.48

4 Results and Discussion

4.1 ANOVA Results

The experimental data of the milling process are shown in Table 2.

The predictive error of the RBF models is assessed based on the coefficients of determination, including R^2, adjusted R^2, and predicted R^2. The R^2 value presents the total variation of the measured data. The adjusted R^2 value represents the total change of the model in terms of the significant factors. The predicted R^2 denotes the accuracy of the formulation for new data. The R^2 values of EF, PO, and R_a are 0.9957, 0.9947, and 0.9938, respectively, which emphasizes the good fitness of the correlations. The adjusted R^2 values of EF, PO, and R_a are 0.9782, 0.9773, and 0.9743, respectively, indicating the adequacy of the models. The predicted R^2 values of EF, PO and R_a are 0.9544, 0.9532, and 0.9523, respectively, indicating the acceptable precision of the formulations, as shown in Fig. 5.

In this paper, the milling trials from 26 to 29 are used to explore the precision of the correlations. The predicted and experimental values are compared at the random points as shown in Fig. 6. The small errors indicate that the RBF models are adequate and can be used for the optimizing process.

Table 3 presents the ANOVA results for the EF model. The p value having less than 0.0001 indicates the significance of the EF model. The factors having p values less 0.05 have statistical contributions on the correlation. The contributions of a, f, V, and r are 43.06%, 26.68%, 19.28%, and 7.50%, respectively, as shown in Fig. 7a. The interaction

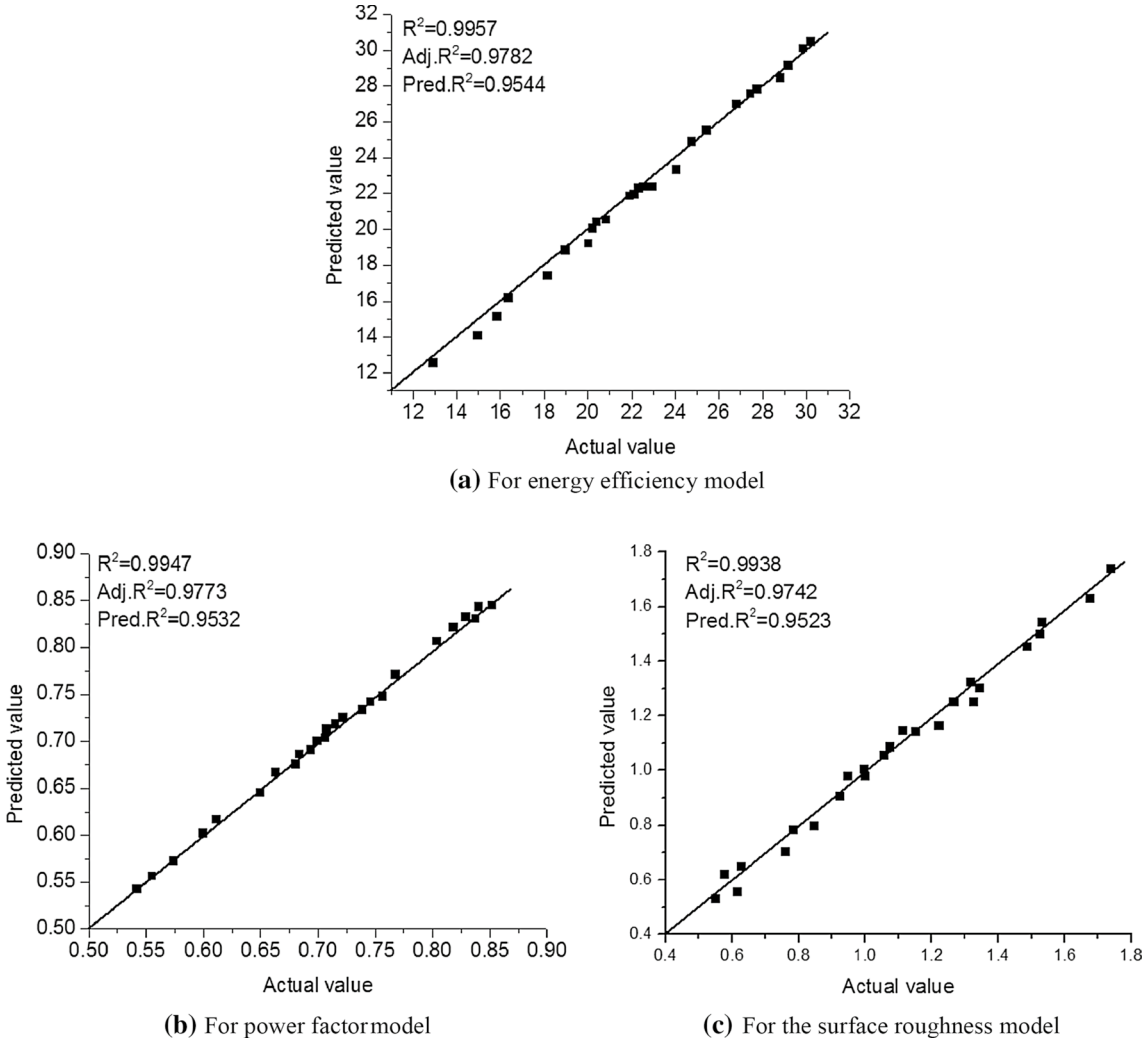

(a) For energy efficiency model

(b) For power factor model

(c) For the surface roughness model

Fig. 5 Evaluation of adequacy of the developed RBF models

terms, including the *Va*, *Vf*, and *ar* are recommended as significant factors. The contributions of the significant quadratic terms, including f^2, a^2, and R^2, are 1.83%, 0.53%, and 0.36%, respectively.

Table 4 presents the ANOVA results for the PO model. The proposed correlation is significant due to the *p* value less than 0.0001. It can be stated that the single terms (*V*, *a*, *f*, and *r*), interactive terms (*Va*, *Vf*, *Vr*, and *fr*), and quadratic terms (V^2 and R^2) are significant factors. The percentage contributions of *a*, *f*, *r*, and *V* are 39.33%, 25.71%, 18.19%, and 14.50%, respectively (Fig. 7b). The contributions of the significant quadratic terms, including r^2 and V^2, are 1.42% and 0.26%, respectively.

Table 5 presents the ANOVA results for the R_a model. The *p* value less than 0.0001 indicates the significance of the R_a model. As a result, the percentage contributions of *a*, *f*, *r*, and *V* are 39.03%, 26.80%, 15.31%, and 12.83%, respectively (Fig. 7c). f^2 is the most influenced factor (4.18%), followed by r^2 (1.14%) for the quadratic terms.

4.2 Effects of Machining Parameters

As shown in Fig. 8, it was pointed out that an increase in the inputs, including the cutting speed, depth of cut, feed rate, and nose radius, leads to higher energy efficiency. The EF value sharply increases when *a* increases from 0.2 to 1.2 mm and *V* changes from 80 to 160 m/min. Additionally, EF significantly improves when *f* increases from 0.03 to 0.1 mm/z and gradually enhances when *r* changes from 0.2 to 0.8 mm.

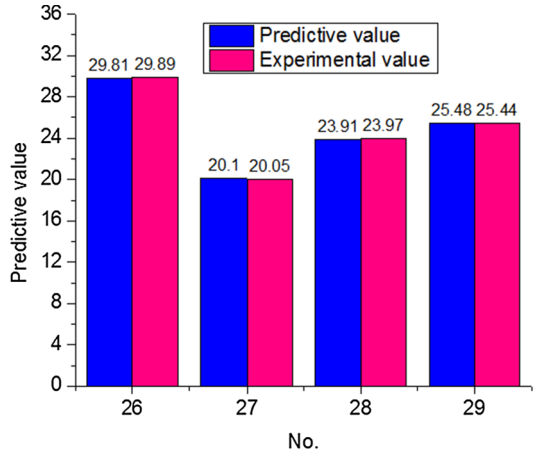

(a) Comparisions for the *EF* model

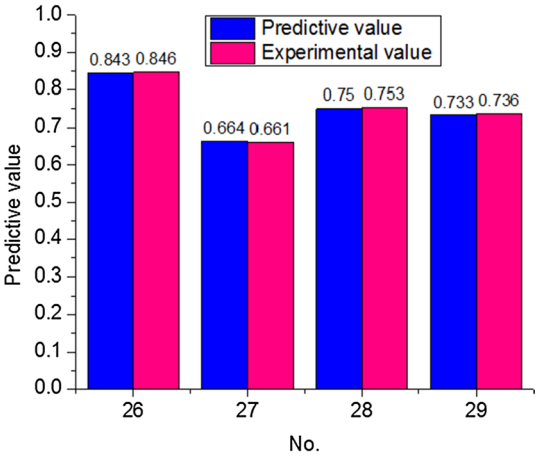

(b) Comparisions for the *PO* model

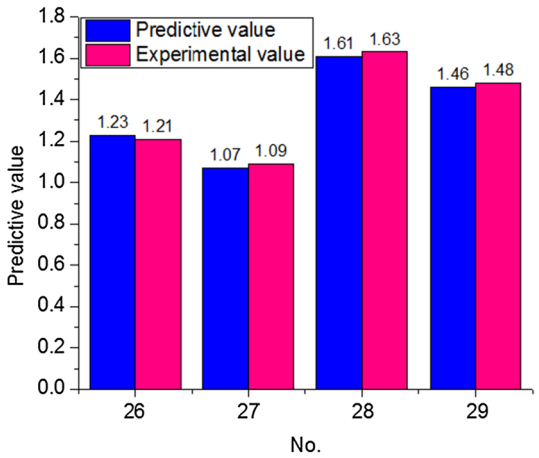

(c) Comparisions for the R_a model

Fig. 6 Comparison between the predicted and experimental values

As cutting speed or spindle speed increases, the power used of the spindle motor increases to improve the speed from the rest to the target value. Moreover, a higher value of the milling momentum on the spindle motor is produced at an increment in the cutting speed. As a result, the active cutting power increases and higher energy efficiency is obtained. Moreover, a higher speed causes an increased temperature in the cutting area and the hardness of the workpiece is decreased, as compared to the initial state. A soft material leads to a reduction in the cutting energy; hence, energy efficiency increases. When V changed from 80 to 160 m/min, EF increased by 29.7% (Fig. 8a).

As depicted in Fig. 8a, an increased depth of cut increases, causing a higher thickness of the un-deformed chip and an increment in the contact area between tool and workpiece. More materials processed result in larger plastic deformation, leading to greater resistance in the milled surface. Therefore, higher active cutting power is required and EF improves. When a changed from 0.2 to 1.2 mm, EF increased by 46.0%.

It can be stated in Fig. 8a that EF increases by an increase in a at a constant value of V. On the other hand, it can be seen that EF enhances by an increment in V at a constant value of a. a is more significant than V for improving energy efficiency.

According to Fig. 8b, when f increases, the reaction forces on the X- and Y-axes of the drive system increase. Therefore, the active cutting power of the drive system increases. Moreover, a higher value of f leads to an increment in the machining temperature on the workpiece surface and may cause the formation of built-up edge (BUE). The BUE results in an increase in the milling force due to a higher contact region between the tool and workpiece; hence, higher active cutting power is consumed. Additionally, the BUE causes an increment in the mechanical strength of the chip due to the work hardening. Obviously, higher active cutting power is required to process material and remove the chip. Consequently, higher energy efficiency is obtained. The EF value increased by 39.9% when f increased from 0.03 to 0.1 mm/z.

Practically, the process parameters, including the cutting speed, feed, and depth of cut, determine the material removal rate value. An increment in the material removal rate requires higher active cutting power. As a result, an increment in energy efficiency is obtained. The maximization of energy efficiency can be observed at the highest MRR.

As depicted in Fig. 8b, a higher value of r causes an increment in the length of the cutting edge, resulting in an increased cutting length between tool and workpiece. More deformed material is produced in the milling time,

Table 3 ANOVA results for the EF model

Source	Sum of squares	Mean square	*F* value	*p* value	Remark	Contri.
Model	582.32,376	41.59455	702.10496	< 0.0001	Significant	
V	91.54133	91.54133	1545.19314	< 0.0001	Significant	19.28
a	204.47212	204.47212	3451.43475	< 0.0001	Significant	43.06
f	126.69301	126.69301	2138.54422	< 0.0001	Significant	26.68
r	35.60408	35.60408	600.98728	< 0.0001	Significant	7.50
Va	0.59290	0.59290	10.00799	0.0101	Significant	0.12
Vf	1.00000	1.00000	16.87973	0.0021	Significant	0.21
Vr	0.01279	0.01279	0.21595	0.6521	Insignificant	0.00
af	0.29160	0.29160	4.92213	0.0508	Insignificant	0.06
ar	1.45086	1.45086	24.49021	0.0006	Significant	0.31
fr	0.13721	0.13721	2.31602	0.1590	Insignificant	0.03
V^2	0.13255	0.13255	2.23739	0.1656	Insignificant	0.03
a^{2t}	2.50373	2.50373	42.26222	< 0.0001	Significant	0.53
f^2	8.68003	8.68003	146.51661	< 0.0001	Significant	1.83
r^2	1.71727	1.71727	28.98704	0.0003	Significant	0.36
Residual	0.59243	0.05924				
Core total	582.91618					

$R^2 = 0.9957$; adjusted $R^2 = 0.9782$; predicted $R^2 = 0.9544$

and a higher degree of plastic deformation is generated. A higher resistance requires more active cutting power to process material and generate a new surface. As a result, EF enhances. The EF value increased by 15.8% when *r* increased from 0.2 to 0.8 mm.

From Fig. 8b, it is seen that irrespective of r, EF increases by an increase in *f*. *f* is more significant than *r* for improving energy efficiency. On the other hand, it can be seen that EF enhances by an increment in *r* at a constant value of *f*. To increase energy efficiency, the values of the processing conditions should have reached the highest level.

As shown in Fig. 9, it can be stated that an increment in the inputs, including the cutting speed, depth of cut, feed rate, and radius, leads to a higher power factor. The PO value significantly enhances when *a* increases from 0.2 to 1.2 mm and *V* changes from 80 to 160 m/min. Additionally, PO sharply increases when *f* increases from 0.03 to 0.1 mm/z and gradually improves when *r* changes from 0.2 to 0.8 mm.

When the cutting speed increases, a higher power of the spindle system is consumed to ensure the rotational motion. A higher acceleration of the spindle motor is required to reach the desired value. Consequently, the active power increases and PO enhances. When *V* changed from 80 to 160 m/min, PO increased by 16.4%.

When the depth of cut increases, a larger contact area between tool and workpiece is generated. A higher value of the material volume is obtained and larger plastic deformation occurs on the machined surface. As a result, a higher active power is consumed to overcome a greater resistance and PO increases. When *a* changed from 0.2 to 1.2 mm, PO increased by 25.5%.

As depicted in Fig. 9a, PO enhances by an increase in *a* at a constant value of *V*. On the other hand, it can be seen that PO enhances by an increment in *V* at a constant value of *a*. The statistical significance of *V* is higher than *a* has for enhancing the power factor.

According to Fig. 9b, when *f* increases, the acceleration of the drive system increases to ensure the setting value of the feed rate. The active power for the *X*- and *Y*-axes also increases to satisfy the machining requirement. Therefore, the active power of the drive system improves and PO improves. The PO value increased by 20.0% when *f* increased from 0.03 to 0.1 mm/z.

As shown in Fig. 9b, a higher value of the radius leads to an increment in cutting length; hence, more material volume is produced. Larger plastic deformation occurs on the workpiece surface. Greater resistance is generated and more active power is required. As a result, PO improves. The PO value increased by 13.0% when *r* increased from 0.2 to 0.8 mm.

From Fig. 9b, it is seen that irrespective of *r*, PO increases by an increase in *f*. *f* is more significant than *r* for improving the power factor. On the other hand, it can be seen that PO enhances by an increment in *r* at a constant value of *f*. To increase the power factor, the values of the processing conditions should have reached the highest level.

Figure 10 depicts the influences of machining parameters on R_a. As shown in Fig. 10a, the reduction in roughness is associated with an increment in *V*. An increased cutting speed leads to an increase in the temperature of the milling region, resulting in a decrease in the strength and hardness of the workpiece. The chip is easily processed

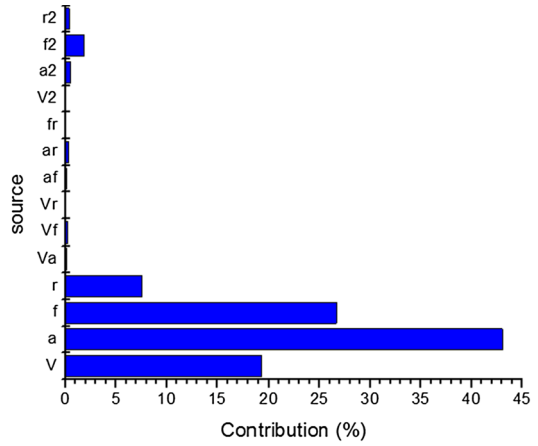

(a) Parametric contribution for the *EF* model

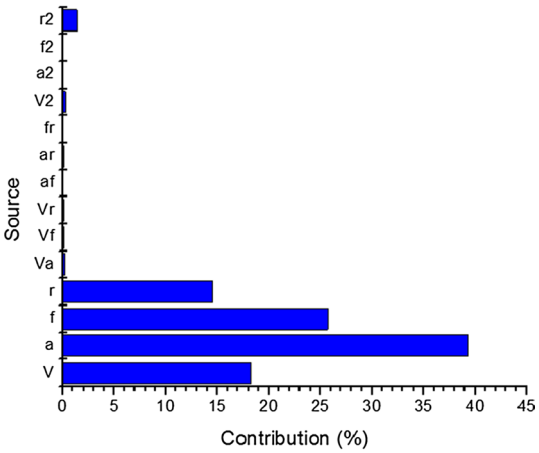

(b) Parametric contribution for the *PO* model

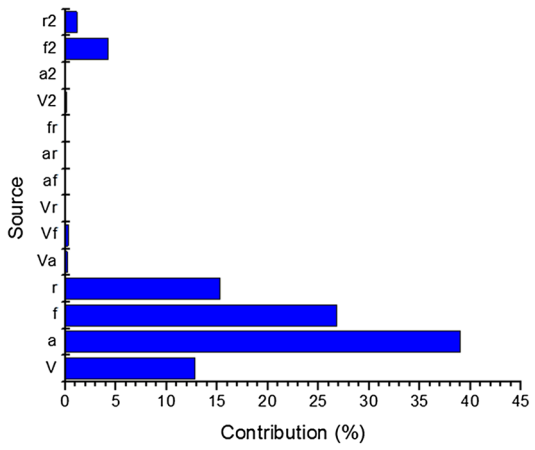

(c) Parametric contribution for the R_a model

Fig. 7 Parametric contribution for the RBF models

from the workpiece surface; hence, a low roughness is produced. A higher value of the cutting speed may decrease the chance of the formation of the BUE and a smoother surface is produced. Moreover, the reduction in the milling force is obtained at a higher value of the cutting speed, which may decrease the machine vibration; hence, a better surface is obtained. The R_a value decreased by 34.6% when V increased from 80 to 160 m/min.

As depicted in Fig. 10a, the increased roughness is associated with an increased depth of cut. When a increases, the contact area between the workpiece and the cutting tool increases, resulting in an increased material removal volume and the milling force. The material heavily is processed from the workpiece surface. This may lead to a chatter in the machine tool, and a higher roughness is produced. The R_a value increased by 103% when a increased from 0.4 to 1.2 mm.

From Fig. 10a, it is seen that irrespective of a, R_a decreases by an increase in V. On the other hand, it can be seen that R_a increases by an increment in a at a constant value of V. a is more significant than V for decreasing roughness. To achieve a smooth surface, the highest value of V is recommended to use, while the lowest level of a should be applied.

As shown in Fig. 10b, an increase in roughness is associated with an increment in f. A low roughness is generated at a low feed rate due to the small distance between the peak and the crest of the milled surface. A higher value of f leads to an increased distance between the milled peaks. Therefore, a higher feed mark is produced on the machined surface and a coarsen surface is generated. Moreover, the BUE generated by a higher feed rate causes the formation of the machined grooves, leading to a reduction in surface quality. The R_a value increased by 62.7% when f increased from 0.03 to 0.10 mm/z.

It is inferred from Fig. 10 that the contact length between the workpiece surface and tool increases when a higher r is used. The height of the roughness profile is reduced, and a smoother surface is produced. Moreover, the chatter could be suppressed due to an increment in stand damping with an increased radius; hence, surface finish is generated. The R_a value decreased by 31.1% when r increased from 0.2 to 0.8 mm.

From Fig. 10b, it is seen that irrespective of f, R_a decreases by an increase in r. On the other hand, it can be seen that R_a increases by an increment in f at a constant value of r. f is more significant than r for decreasing roughness. To achieve a smooth surface, the highest value of r is recommended to use, while the lowest level of f should be applied.

Table 4 ANOVA results for the PO model

Source	Sum of squares	Mean square	*F* value	*p* value	Remark	Contri.
Model	0.193485	0.013820	806.241753	< 0.0001	Significant	
V	0.030038	0.030038	1752.338037	< 0.0001	Significant	18.19
a	0.064927	0.064927	3787.650884	< 0.0001	Significant	39.33
f	0.042441	0.042441	2475.904481	< 0.0001	Significant	25.71
r	0.023941	0.023941	1396.674769	< 0.0001	Significant	14.50
Va	0.000361	0.000361	21.059796	0.0010	Significant	0.22
Vf	0.000210	0.000210	12.265435	0.0057	Significant	0.13
Vr	0.000184	0.000184	10.730223	0.0083	Significant	0.11
af	0.000025	0.000025	1.458435	0.2550	Insignificant	0.02
ar	0.000163	0.000163	9.495583	0.0116	Significant	0.10
fr	0.000020	0.000020	1.154846	0.3078	Insignificant	0.01
V^2	0.000424	0.000424	24.717893	0.0006	Significant	0.26
a^2	0.000010	0.000010	0.579084	0.4642	Insignificant	0.01
f^2	0.000001	0.000001	0.041179	0.8433	Insignificant	0.00
r^2	0.002352	0.002352	137.205100	< 0.0001	Significant	1.42
Residual	0.000171	0.000017				
Core total	0.193656					

$R^2 = 0.9947$; adjusted $R^2 = 0.9773$; predicted $R^2 = 0.9532$

Table 5 ANOVA results for the R_a model

Source	Sum of squares	Mean square	*F* value	*p* value	Remark	Contri.
Model	3.02631	0.21616	47.95672	< 0.0001	Significant	
V	0.34102	0.34102	75.65579	< 0.0001	Significant	12.83
a	1.03723	1.03723	230.11185	< 0.0001	Significant	39.03
f	0.71240	0.71240	158.04772	< 0.0001	Significant	26.80
r	0.40701	0.40701	90.29580	< 0.0001	Significant	15.31
Va	0.00490	0.00490	1.08708	0.3217	Insignificant	0.18
Vf	0.00722	0.00722	1.60288	0.2342	Insignificant	0.27
Vr	0.00019	0.00019	0.04310	0.8397	Insignificant	0.01
af	0.00122	0.00122	0.27177	0.6135	Insignificant	0.05
ar	0.00017	0.00017	0.03672	0.8519	Insignificant	0.01
fr	0.00145	0.00145	0.32137	0.5833	Insignificant	0.05
V^2	0.00261	0.00261	0.57954	0.4641	Insignificant	0.10
a^2	0.00108	0.00108	0.24023	0.6346	Insignificant	0.04
f^2	0.11107	0.11107	24.64041	0.0006	Significant	4.18
r^2	0.03018	0.03018	6.69462	0.0271	Significant	1.14
Residual	0.04508	0.00451				
Core total	3.07138					

$R^2 = 0.9938$; adjusted $R^2 = 0.9743$; predicted $R^2 = 0.9523$

The machined surfaces at various machining inputs are shown in Fig. 11. The milled faults, including the grooves, cracks, and voids, are produced at a higher depth of cut (Fig. 11a). A smoother surface is obtained at a low condition, as shown in Fig. 11b.

The wears of the cutting inserts at different inputs are depicted in Fig. 12 [24]. As depicted in Fig. 12a, the smooth abrasion mark is produced on the rake face at a low value of the depth of cut to the abrasive mechanism and the adhesion of the material. The crater wear on the cutting edge is observed at a higher value of the depth of cut, as shown in Fig. 12b. The hardness and strength of the insert decreased due to higher pressure and temperature.

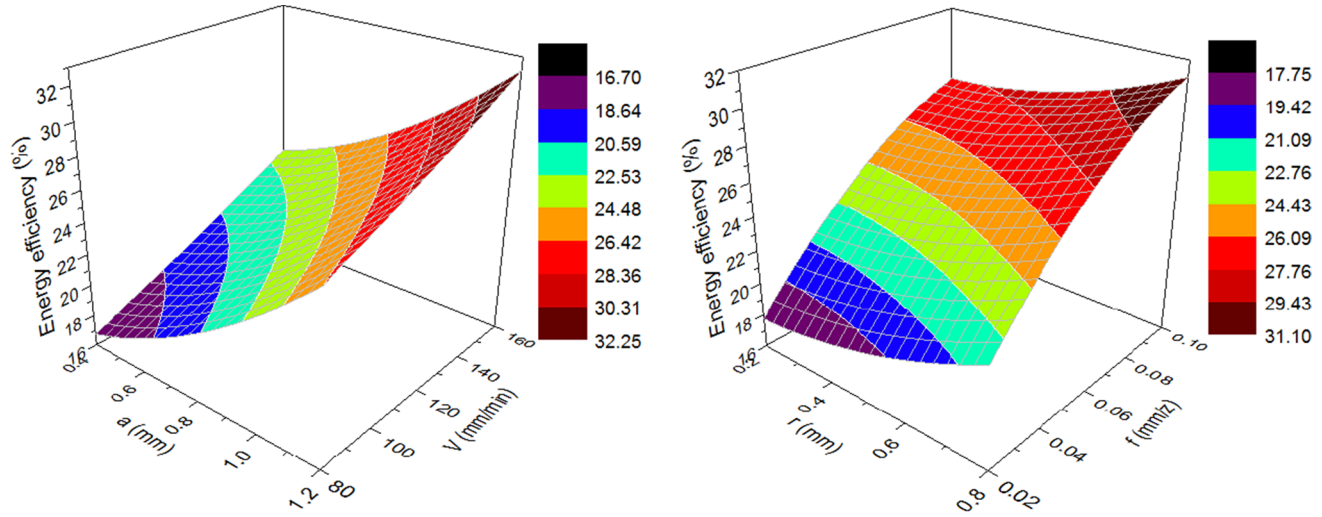

(a) *EF* versus *V* and *a* **(b)** *EF* versus *r* and *f*

Fig. 8 Interaction effects of the machining parameters on the EF model

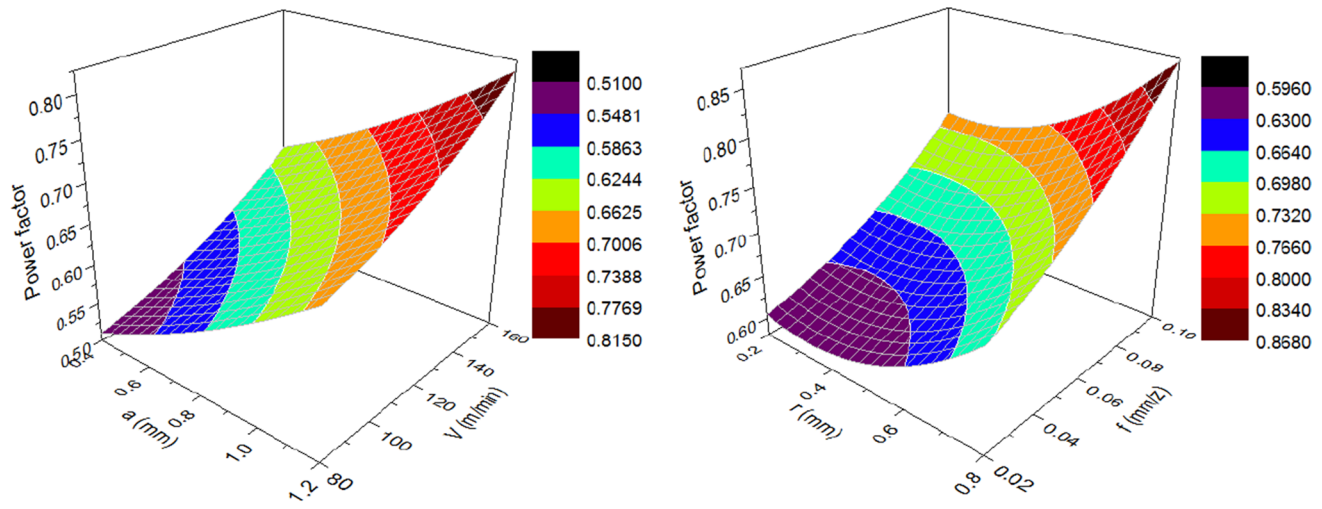

(a) *PO* versus *V* and *a* **(b)** *PO* versus *r* and *f*

Fig. 9 Interaction effects of the machining parameters on the PO model

4.3 Optimization Results

The developed equations showing the relationship between process parameters and machining responses are used to find optimal parameters with the aid of the ASA. The optimal point with blue color is shown in Fig. 13. The optimization results are listed in Table 6. As a result, the reduction in R_a is 39.18%, while EF and PO increase around 26.47% and 22.61%, respectively, as compared to the initial values.

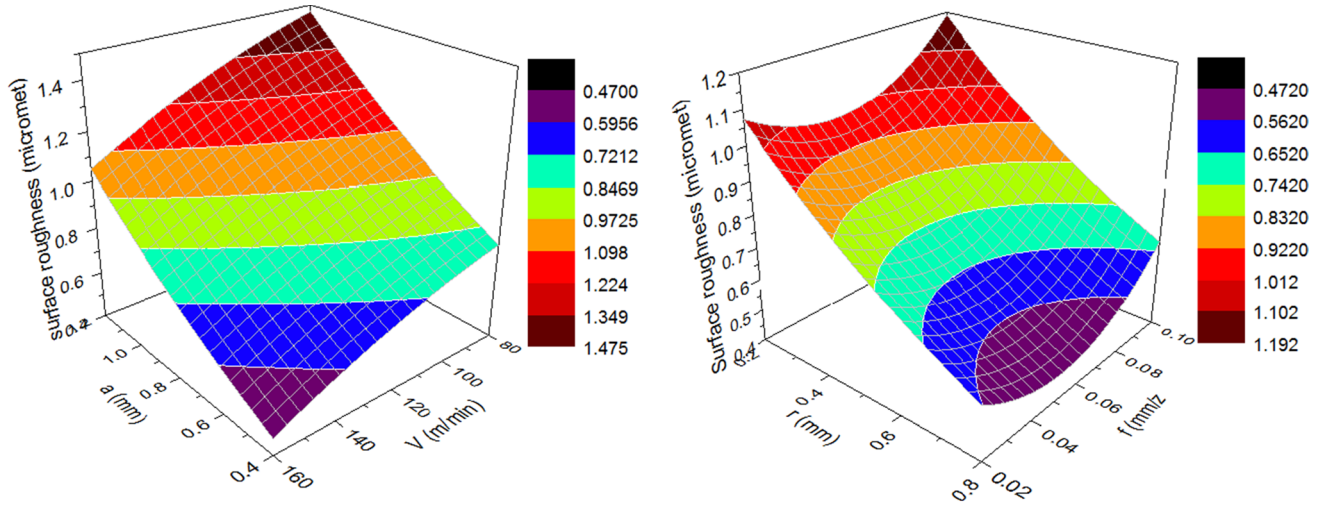

(a) R_a versus f and a **(b)** R_a versus r and V

Fig. 10 Interaction effects of the machining parameters on the R_a model

Fig. 11 Milled surfaces at different inputs

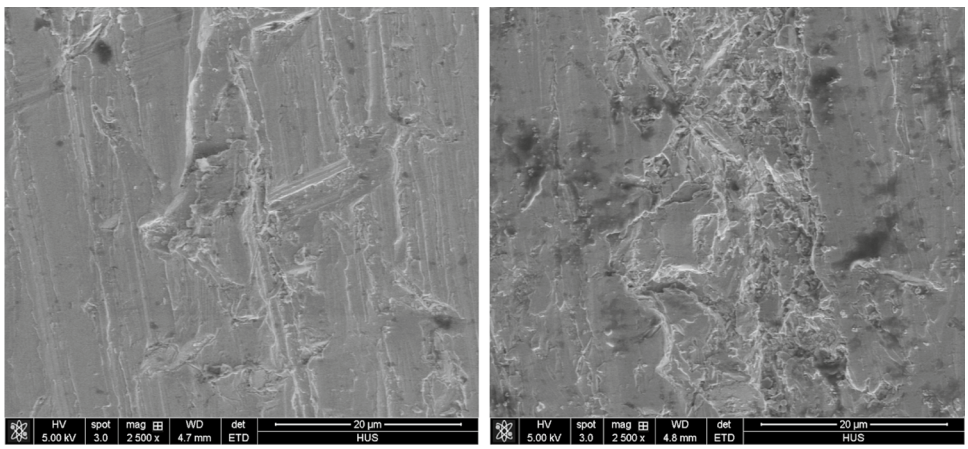

(a) Milled surface at experimental No. 4 **(b)** Milled surface at experimental No.24

Fig. 12 The tool wear at different inputs

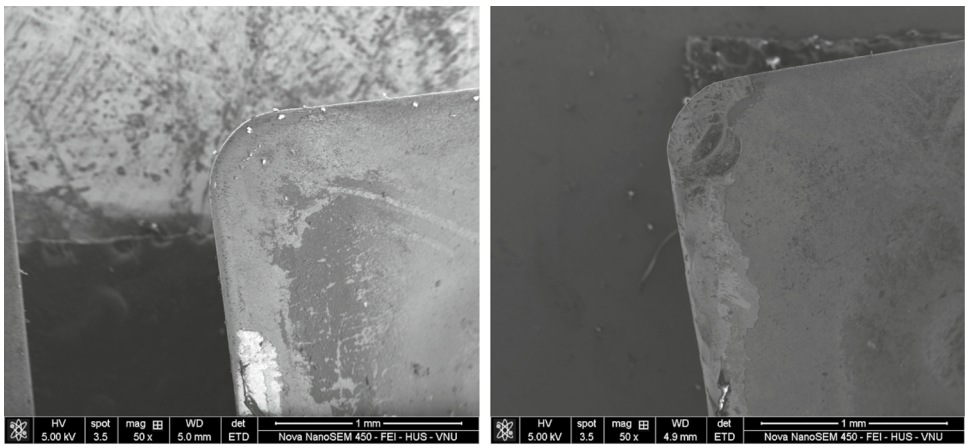

(a) The tool wear at experimental No. 17 **(b)** The tool wear at experimental No. 7

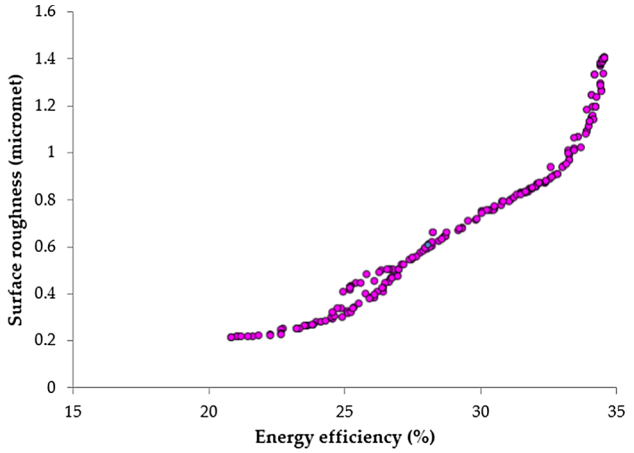

(a) EF and R_a

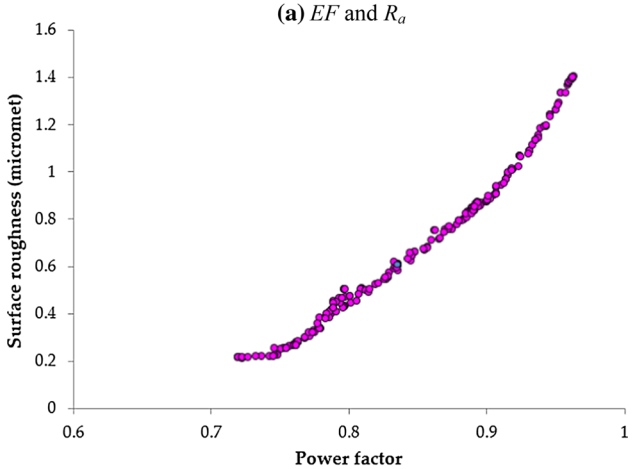

(b) PF and R_a

Fig. 13 Pareto fronts generated by the ASA

5 Conclusions

In the current work, the machining parameters, including the cutting speed, the feed, the depth of cut, and the nose radius, were optimized to enhance the energy efficiency, power factor, and roughness. The formulations between the inputs and outputs were constructed by means of the RBF models. The statistical significance was assessed employing ANOVA. The ASA was used to predict the optimal values. The main findings of this research can be listed as follows:

1. It can be stated that the inputs have significant contributions to the milling responses. An increment in energy efficiency and/or power factor was obtained at high values of the inputs. A better surface was produced at high values of the cutting speed and radius. To decrease the roughness, lower values of a depth of cut or feed rate should be used. The ANOVA results indicated that the milling performances are primarily affected by a, f, V, and r, respectively.
2. The correlations of EF, PO, and R_a were developed to explore the influences of the inputs on the milling performances. The proposed formulations are recommended to use for predicting the technical outputs before the experiments because of the high values of the evaluating coefficients.
3. The best milling performances were achieved at V of 160 m/min, a of 0.08 mm, f of 0.07 mm/z, and r of 0.8 mm. The enhanced values of EF and PO are 26.47% and 22.61%, respectively, while R_a decreases approximately 39.18% at the optimal point.
4. The Pareto fronts generated by the ASA can significantly support the milling operators to select appropriate parameters to maximize the power factor as well as energy efficiency and minimize the surface roughness. The selection of optimal parameters can decrease the efforts required and machining costs as well as time. The hybrid approach consisting of the RBF models and ASA can widely apply for the optimization of the milling process instead of using human experience.
5. The main findings of this work can be considered as an effective solution in the face milling process, especially when energy efficiency and machined quality are required. The future work may deal with the impacts of the inputs on the production costs.

Table 6 Optimization results using ASA

Method	Optimization parameters				Responses		
	V (m/min)	a (mm)	f (mm/z)	r (mm)	PO	EF (%)	R_a (μm)
Initial	120	0.80	0.07	0.4	0.681	22.14	0.97
ASA	160	0.85	0.06	0.8	0.835	28.00	0.59
Improvement (%)					22.61	26.47	− 39.18

Acknowledgements This research is funded by Vietnam National Foundation for Science and Technology Development (NAFOSTED) under Grant Number 107.04-2020.02

References

1. Ryzhkin, A.A.; Shuchev, K.G.; Aliev, M.M.; Gusev, V.V.: Dissipative properties of lubricant and coolant fluid in cutting and friction. Russ. Eng. Res. **28**, 1243–1247 (2008)
2. Aydın, M.; Karakuzu, C.; Uçar, M.; Cengiz, A.; Çavuşlu, M.A.: Prediction of surface roughness and cutting zone temperature in dry turning processes of AISI304 stainless steel using ANFIS with PSO learning. Int. J. Adv. Manuf. Technol. **67**, 957–967 (2013)
3. Shihab, S.K.; Khan, Z.A.; Mohammad, A.; Siddiquee, A.N.: Optimization of surface integrity in dry hard turning using RSM. Sadhana **39**, 1035–1053 (2014)
4. Mia, M.; Dhar, N.R.: Modeling of surface roughness using RSM, FL and SA in dry hard turning. Arab. J. Sci. Eng. **43**, 1125–1136 (2018)
5. Angappan, P.; Thangiah, S.; Subbarayan, S.: Taguchi-based grey relational analysis for modeling and optimizing machining parameters through dry turning of Incoloy 800H. J. Mech. Sci. Technol. **31**, 4159–4165 (2017)
6. Zerti, O.; Yallese, M.A.; Khettabi, R.; Chaoui, K.; Mabrouki, T.: Design optimization for minimum technological parameters when dry turning of AISI D3 steel using Taguchi method. Int. J. Adv. Manuf. Technol. **89**, 1915–1943 (2017)
7. Tamang, S.K.; Chandrasekaran, M.; Sahoo, A.K.J.: Sustainable machining: an experimental investigation and optimization of machining Inconel 825 with dry and MQL approach. Braz. Soc. Mech. Sci. Eng. **40**, 374 (2018)
8. Al-Zubaidi, S.; Ghani, J.A.; Che Haron, C.H.: Prediction of tool life when end milling of Ti6Al4V alloy using hybrid learning system. Arab. J. Sci. Eng. **39**, 5095–5111 (2014)
9. Karabulut, Ş.; Gökmen, U.; Çinici, H.: Optimization of machining conditions for surface quality in milling AA7039-based metal matrix composites. Arab. J. Sci. Eng. **43**, 1071–1082 (2018)
10. Li, H.; He, G.; Qin, X.; Wang, G.; Lu, C.; Gui, L.: Tool wear and hole quality investigation in dry helical milling of Ti–6Al–4V alloy. Int. J. Adv. Manuf. Technol. **71**, 1511–1523 (2014)
11. Le Coz, G.; Dudzinski, D.: Temperature variation in the workpiece and in the cutting tool when dry milling Inconel 718. Int. J. Adv. Manuf. Technol. **74**, 1133–1139 (2014)
12. Jomaa, W.; Lévesque, J.; Bocher, P.; et al.: Optimization study of dry peripheral milling process for improving aeronautical part integrity using grey relational analysis. Int. J. Adv. Manuf. Technol. **91**, 931–942 (2017)
13. Khettabi, R.; Nouioua, M.; Djebara, A.; Songmene, V.: Effect of MQL and dry processes on the particle emission and part quality during milling of aluminum alloys. Int. J. Adv. Manuf. Technol. **92**, 2593–2598 (2017)
14. Safari, H.; Sharif, S.; Izman, S.; Jafari, H.: Surface integrity characterization in high-speed dry end milling of Ti–6Al–4V titanium alloy. Int. J. Adv. Manuf. Technol. **78**, 651–657 (2015)
15. Shi, K.; Zhang, D.; Ren, J.: Optimization of process parameters for surface roughness and microhardness in dry milling of magnesium alloy using Taguchi with grey relational analysis. Int. J. Adv. Manuf. Technol. **81**, 645–651 (2015)
16. Karabulut, Ş.; Çinici, H.; Karakoç, H.: Experimental investigation and optimization of cutting force and tool wear in milling Al7075 and open-cell SiC foam composite. Arab. J. Sci. Eng. **41**, 1797–1912 (2016)
17. Baowan, P.; Saikaew, C.; Wisitsoraat, A.: Influence of helix angle on tool performances of TiAlN- and DLC-coated carbide end mills for dry side milling of stainless steel. Int. J. Adv. Manuf. Technol. **90**, 3085–3097 (2017)
18. Campatelli, G.; Lorenzini, L.; Scippa, A.: Optimization of process parameters using a response surface method for minimizing power consumption in the milling of carbon steel. J. Clean. Prod. **66**, 309–316 (2014)
19. Yang, Y.; Li, X.; Gao, L.; Sao, X.: Modeling and impact factors analyzing of energy consumption in CNC face milling using GRASP gene expression programming. Int. J. Adv. Manuf. Technol. **87**, 1247–1263 (2016)
20. Zhang, H.; Deng, S.; Fu, Y.; Lishu, L.; Yan, C.: A process parameters optimization method of multi-pass dry milling for high efficiency, low energy and low carbon emissions. J. Clean. Prod. **148**, 174–184 (2017)
21. Bilga, P.S.; Singh, S.; Kumar, R.: Optimization of energy consumption response parameters for turning operation using Taguchi method. Clean. Prod. **137**, 1406–1417 (2016)
22. Shihab, S.K.: Optimization of WEDM process parameters for machining of friction-stir-welded 5754 aluminum alloy using box-behnken design of RSM. Arab. J. Sci. Eng. **43**, 5017–5027 (2018)
23. Keshtegara, B.; Mert, C.; Kisic, O.: Comparison of four heuristic regression techniques in solar radiation modeling: Kriging method vs RSM, MARS and M5 model tree. Renew. Sustain. Energy Rev. **2018**(81), 330–341 (2018)
24. Huibin, S.; Dali, C.; Zidong, Zh; Xia, K.: A hybrid approach to cutting tool remaining useful life prediction based on the Wiener process. IEEE T. Reliab. **67**, 1294–1303 (2018)